3D Electromagnetic Imaging Using Compressive Sensing

Marija Nikolic, Gongguo Tang, Arye Nehorai
Department of Electrical and Systems Engineering
Washington University in St. Louis
St. Louis, MO 63130-1127
Email: nehorai@ese.wustl.edu

***Abstract*—We develop the application of compressive sensing (CS) for solving general inverse electromagnetic problems such as three-dimensional (3D) microwave imaging. The goal is to estimate locations of unknown, but sparse targets, hidden inside dielectric bodies. The potential of CS for localizing sparse targets in vacuum or buried in ground was shown in previous work. We extend the proposed schemes by considering arbitrary embedding medium and exploiting dual-polarized measurements. We compare the performance of CS and beamforming in the breast-cancer estimation problem.**

***Index Terms*—breast cancer, compressive sensing, sparse signal processing, microwave imaging, radar, inverse scattering**

I. Introduction

We consider the application of compressive sensing (CS) for solving general inverse electromagnetic problems such as localizing targets hidden inside dielectric bodies using sparse signal reconstruction and far-field electromagnetic measurements. This is typically an ill-posed problem unless some prior knowledge about targets or environment is available. We show that the positions of targets with arbitrary shapes are reliably reconstructed if they are sparse within the dielectric body, and if their electromagnetic properties sufficiently differ from the surrounding environment.

Sparse signal reconstruction aims at recovering a sparse signal from linear measurements of a usually underdetermined system. More precisely, suppose we have a k-sparse signal $\boldsymbol{x} \in \mathbb{F}^n$, that is, $\boldsymbol{x}$ has at most k non-zero components. We observe $\boldsymbol{y} \in \mathbb{F}^m$ through the following linear system:

$$\boldsymbol{y} = A\boldsymbol{x} + \boldsymbol{e}, \tag{1}$$

where $A \in \mathbb{F}^{m\times n}$ is the measurement/sensing matrix and $\boldsymbol{e} \in \mathbb{F}^m$ is the noise vector. The measurement system is underdetermined because $m \ll n$ in general. This measurement model gained popularity in recent years due to the growing interest in CS [1], [2], a new framework for compression, sensing, and sampling that promises to break the sampling limit set by Shannon and Nyquist. Consider the noise-free case. Ideally, we would like to exploit the sparsity of $\boldsymbol{x}$ and reconstruct $\boldsymbol{x}$ through solving the following, unfortunately, NP-hard optimization problem:

$$\min \|\boldsymbol{x}\|_0 \quad \text{subject to} \quad \boldsymbol{y} = A\boldsymbol{x}. \tag{2}$$

A major advance in sparse signal reconstruction is that we can actually replace the ℓ_0 norm with the convex ℓ_1 norm and can still recover $\boldsymbol{x}$ under certain conditions. This convex relaxation technique is employed in several very successful algorithms for sparse signal reconstruction, *e.g.,* basis pursuit [3], Dantzig selector [4] and LASSO estimator [5]. These algorithms can be applied to the noisy case as well.

The application of sparse signal processing for estimating point targets in vacuum was investigated in [15]. Recently, the field of CS was extended to inverse problems such as detecting buried targets using ground penetrating radar (GPR) [16], and through-the-wall imaging [17]. The linkage between CS and random arrays was established in [18].

Here, we extend the application of CS for estimating targets embedded in arbitrary 3D dielectric body of known electromagnetic properties. We develop statistical models that exploit the information content of ultra-wideband (UWB) measurements and dual polarization. We show the large potential of CS in solving important real-life problems such as breast-tumor detection. In the analyzed example, we use realistic models that take into account dispersive breast-tissue parameters and antenna array properties.

II. Measurement Model

We assume an array of M antennas placed above the dielectric body under inspection (Fig. 1). The goal is to estimate the position of inhomogeneities (targets) inside the domain of, otherwise, known electromagnetic properties. The inhomogeneities are supposed to occupy a small portion of the body, with electromagnetic characteristics different from the surrounding dielectric.

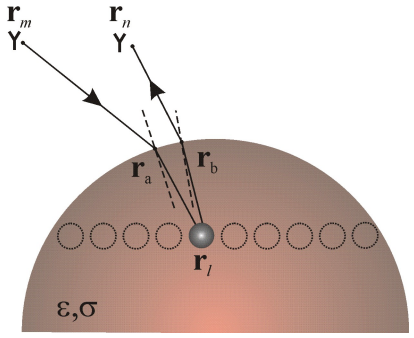

Fig. 1. Transmitter-receiver pair and the dielectric body with a target inside.

We adopt a measurement scheme in which all antennas transmit and receive electromagnetic pulses. The antennas in

This work was supported by the Department of Defense under the Air Force Office of Scientific Research MURI Grant FA9550-05-1-0443, and ONR Grant N000140810849.

the array are sensitive to both vertical and horizontal polarization, and they are positioned at $\boldsymbol{r}_m, m = 1, \ldots, M$. We search for targets at L candidate locations, $\boldsymbol{r}_l, l = 1, \ldots, L$. If the array is in the far field of the dielectric body and its dimensions are large compared with the wavelength, the signal observed at the nth sensor due to a target at the lth location when the mth sensor is excited, approximately, reads:

$$Y^l_{mn}(f_i) = \frac{x_l}{S^l_{mn}} \exp\Big[-jk_0 \left(|\boldsymbol{r}_m - \boldsymbol{r}_a| + |\boldsymbol{r}_n - \boldsymbol{r}_b|\right) -jk \left(|\boldsymbol{r}_a - \boldsymbol{r}_l| + |\boldsymbol{r}_b - \boldsymbol{r}_l|\right)\Big] G(f_i) + E + C \quad (3)$$

with

$$k = k_0 \sqrt{\varepsilon_r - j\frac{\sigma}{2\pi f_i}}, k_0 = \frac{2\pi f_i}{c_0} \text{ and } S^l_{mn} = S^l_m S^l_n, \quad (4)$$

for $m, n = 1, \ldots, M,\ i = 1, \ldots, I,\ l = 1, \ldots, L$. Here x_l is the target scattering coefficient, $\boldsymbol{r}_m$ and $\boldsymbol{r}_n$ are the sensor locations, $\boldsymbol{r}_a$ and $\boldsymbol{r}_b$ the refraction points (Fig. 1), and $\boldsymbol{r}_l$ is the target location. S^l_{mn} is the spatial attenuation (spreading factor), and k and k_0 are the propagation constants in dielectric and vacuum, respectively. The permittivity of the dielectric is ϵ and conductivity is σ. Finally, G is the waveform, E is additive noise, and C is the clutter. The main sources of the clutter are unwanted reflections from the air-dielectric boundary. The clutter is usually eliminated in the time domain using windowing or FIR-filter (e.g., [11]). In the following analysis we assume that the unwanted reflections are removed from the observed signal and that signal is corrupted only by additive white Gaussian noise. The measurement equation in the time-domain reads

$$y^l_{mn}(t) = \tilde{g}^l_{mn}(t) + e(t) \quad (5)$$

where

$$\tilde{g}^l_{mn}(t) = F^{-1}\Bigg\{ \frac{x_l}{S^l_{mn}} \exp\Big[-jk_0 \left(|\boldsymbol{r}_m - \boldsymbol{r}_a| + |\boldsymbol{r}_n - \boldsymbol{r}_b|\right) -jk \left(|\boldsymbol{r}_a - \boldsymbol{r}_l| + |\boldsymbol{r}_b - \boldsymbol{r}_l|\right)\Big] G(f_i)\Bigg\} \quad (6)$$

with $F^{-1}(\cdot)$ the inverse Fourier transformation. In the spirit of sparse signal reconstruction, the observed signal may be written as

$$y_{mn}(t) = \left[\ \tilde{g}^1_{mn}(t) \quad \ldots \quad \tilde{g}^L_{mn}(t)\ \right] \begin{bmatrix} x_1 \\ \vdots \\ x_L \end{bmatrix} + e_{mn}(t), \quad (7)$$

where the number of nonzero scattering coefficients is small with respect to the number of candidate target locations. When the multiple temporal samples are present, (7) becomes

$$\boldsymbol{y}_{mn} = G_{mn}\boldsymbol{x} + \boldsymbol{e}_{mn} \quad (8)$$

with

$$\boldsymbol{y}_{mn} = \left[\ y_{mn}(t_1) \quad \ldots \quad y_{mn}(t_N)\ \right]^T, \quad (9)$$

$$G_{mn} = \begin{bmatrix} \tilde{g}^1_{mn}(t_1) & \ldots & \tilde{g}^L_{mn}(t_1) \\ \vdots & \ddots & \vdots \\ \tilde{g}^1_{mn}(t_N) & \ldots & \tilde{g}^L_{mn}(t_N) \end{bmatrix}, \quad (10)$$

$$\boldsymbol{x} = \left[\ x_1 \quad \ldots \quad x_L\ \right]^T, \quad (11)$$

$$\boldsymbol{e}_{mn} = \left[\ e_{mn}(t_1) \quad \ldots \quad e_{mn}(t_N)\ \right]^T, \quad (12)$$

where N is the number of temporal samples. We stack the measurements observed by different transmitting-receiving pairs:

$$\begin{bmatrix} \boldsymbol{y}_{11} \\ \boldsymbol{y}_{12} \\ \vdots \\ \boldsymbol{y}_{MM} \end{bmatrix} = \begin{bmatrix} G_{11} \\ G_{12} \\ \vdots \\ G_{MM} \end{bmatrix} \begin{bmatrix} x_1 \\ x_2 \\ \vdots \\ x_L \end{bmatrix} + \begin{bmatrix} \boldsymbol{e}_{11} \\ \boldsymbol{e}_{12} \\ \vdots \\ \boldsymbol{e}_{MM} \end{bmatrix}, \quad (13)$$

or equivalently in the matrix form

$$\boldsymbol{y}^{h(v)} = G\boldsymbol{x}^{h(v)} + \boldsymbol{e}^{h(v)}. \quad (14)$$

where the superscripts v and h correspond to vertical and horizontal polarization. We include both polarizations in the model (14):

$$\begin{bmatrix} \boldsymbol{y}^v \\ \boldsymbol{y}^h \end{bmatrix} = \begin{bmatrix} G^{vv} & G^{vh} \\ G^{hv} & G^{hh} \end{bmatrix} \begin{bmatrix} \boldsymbol{x}^v \\ \boldsymbol{x}^h \end{bmatrix} + \begin{bmatrix} \boldsymbol{e}^v \\ \boldsymbol{e}^h \end{bmatrix}, \quad (15)$$

or compactly

$$\boldsymbol{y} = G\boldsymbol{x} + \boldsymbol{e}. \quad (16)$$

The scattering vector $\boldsymbol{x}$ is sparse in the domain of target locations. We define the ℓ_2-norm of scattering coefficient at the lth candidate target location as

$$x^{(\ell_2)}_l = \sqrt{(x^v_l)^2 + (x^h_l)^2}. \quad (17)$$

To recover the true target positions inside the dielectric we use the LASSO estimator [5]

$$\hat{\boldsymbol{x}} = \text{argmin}_{\boldsymbol{x}} \|\boldsymbol{y} - G\boldsymbol{x}\|_2 + \lambda \|\boldsymbol{x}^{(\ell_2)}\|_1 \quad (18)$$

where $\boldsymbol{x}^{(\ell_2)} = \left[\ x^{(\ell_2)}_1 \quad \ldots \quad x^{(\ell_2)}_L\ \right]$. Since the noise $\boldsymbol{e}$ is usually unbounded, the LASSO estimator is more appropriate than the Basis Pursuit algorithm [3], which applies to the noise-free case and the bounded noise case. In future work, we will also apply the Dantzig Selector proposed in [4] and compare its results with those given by the LASSO estimator.

We use the ray tracing to compute (3). We apply the Snell's law on the surface of the outer dielectric, approximated by a quadrilateral mesh, to find the refraction points. Since this computation is not analytically tractable, we resort to the simplex optimization. The attenuation and distortion of the signal due to the losses in the dielectric are included through the complex propagation constant. We also determine numerically the spreading factor in (3) as the ratio of the cross-sectional areas of the ray tube at the target location S_2 and that at the reference distance in vacuum S_1 [6], as shown in Fig. 2. To solve problem (18) we used CVX [19], a package for specifying and solving convex programs [20].

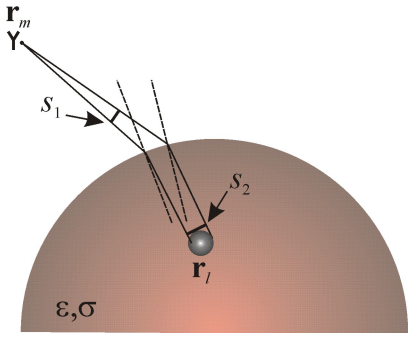

Fig. 2. Spreading factor computation.

III. Breast Tumor Localization

We apply the results developed in the previous section to compute high-resolution images of breast cancer. Recent investigations showed that microwave imaging is a promising technique for an early-stage detection of breast cancer [7], [10]. Main approaches in this area are microwave tomography [7], [8], [9] and radar imaging [10], [11], [12], [13]. Microwave tomography reconstructs a complete dielectric body from the scattered field, which is a computationally demanding and ill-posed inverse problem. In radar imaging, as in CS, the focus is on localizing targets rather then estimating the whole domain. We compare the results of CS with those obtained by beamforming that is a standard imaging technique [11], [12]. We follow the model described in [13]. The breast is considered as a homogeneous dielectric body in the shape of paraboloid with parameters: $a = 5\text{cm}$, $b = 5\text{cm}$, and $c = 6\text{cm}$. The relative permittivity of the breast tissue is $\epsilon_r = 10$ and the conductivity is $\sigma = 0.15\text{S/m}$. Tumor shapes vary from smooth spherical bodies to the complex star-like shapes. The relative permittivity of the tumors is $\epsilon_r = 51$ and the conductivity $\sigma = 4.8\text{S/m}$. We suppose two star-shaped tumors centered at $(1\text{cm}, 0, 3\text{cm})$ and $(2\text{cm}, 0, 2\text{cm})$, with circumscribed radius $R = 3\text{mm}$ (Fig. 3).

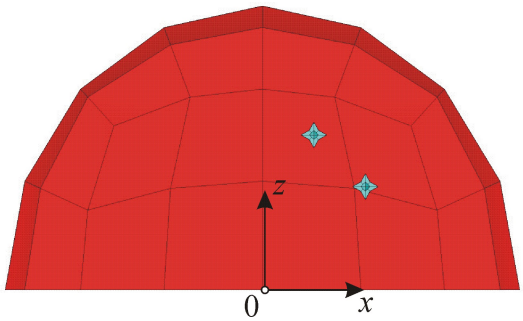

Fig. 3. Cross-section of the breast model with tumors.

We assume that the measurements are taken by the array of cone dipoles (arm height $h = 1\text{cm}$, cone radius $r = 1\text{cm}$). Dipoles form a uniform 4×4 planar array, where the separation between adjacent array elements is 6cm, as shown in Fig. 4. The dual polarization is achieved by rotating the array for $90°$. The array elements are excited by a modulated Gaussian pulse centered at $f_0 = 6\text{GHz}$. The unmodulated pulse in the time-domain is $h(t) = e^{-(t/\tau)^2}$, $\tau = 0.15\text{ns}$. We use 3D-MoM electromagnetic solver WIPL-D [14] to determine the array response (s-matrix). Computations are performed for all frequencies in the range $f \in [2\text{GHz}, 12\text{GHz}]$,with the frequency step $\Delta f = 50\text{MHz}$. Measurements are corrupted by additive white Gaussian noise, with the adopted $\text{SNR} = 10\text{dB}$.

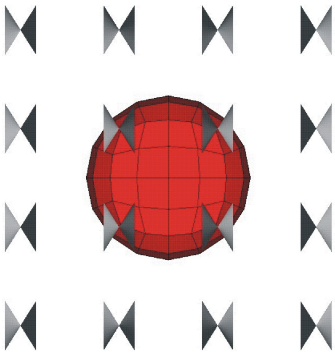

Fig. 4. Array of conical dipoles above the breast model.

The shape of the transmitted waveform G depends on the sensors. For given array, we compute the waveform numerically using [14] in the frequency domain as

$$G(f) = S_{12}(f)H(f)\exp(\jmath 2\pi f/c_0) \tag{19}$$

where S_{12} is the s-coefficient between two antennas in vacuum separated by $d = 1\text{m}$ and $H(f)$ is the Fourier transform of unmodulated pulse $h(t)$. The exponential term centers the waveform at $t = 0$. We denote the Inverse Fourier transform of (19) as the reference waveform, $g(t)$.

We show the results of the breast-cancer estimation using CS and single polarization in Fig. 5. Targets are well resolved and the brightest spots correspond to their true locations. The estimation is further improved if both polarizations are included, as we show in Fig. 6. (In the computations we set $\lambda = 1$.) For a comparison, we solve the same problem by beamforming. In the beamforming, measurements taken at different sensor positions are aligned in time and summed for each candidate location:

$$y(t, \boldsymbol{r}_l) = \sum_{m,n} y^l_{mn}(t + \tau^l_{mn}) \tag{20}$$

with

$$\tau^l_{mn} = (|\boldsymbol{r}_m - \boldsymbol{r}_a| + |\boldsymbol{r}_n - \boldsymbol{r}_b| + \sqrt{\epsilon_r}(|\boldsymbol{r}_a - \boldsymbol{r}_l a| + |\boldsymbol{r}_b - \boldsymbol{r}_l|)/c_0) \tag{21}$$

The intensity at the lth pixel is computed by correlating the aligned signal with the reference waveform

$$I(\boldsymbol{r}_l) = \int_0^T y(t, \boldsymbol{r}_l)g(t)\mathrm{d}t. \tag{22}$$

The pixels with maximal intensities are supposed to be at the true target locations. In Fig. 7 we show the result of the beamforming applied to single-polarized measurements. The computed image is blurred with large overlapping target spreads, in contrast to the case shown in Fig. 5.

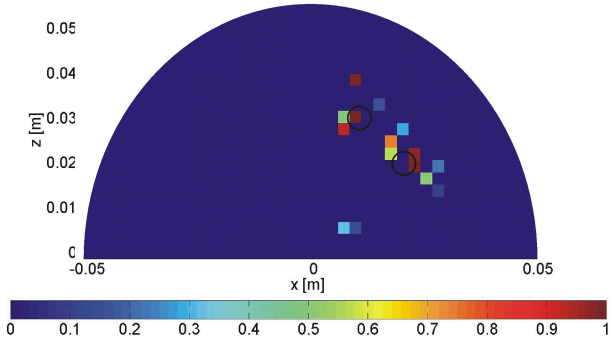

Fig. 5. Breast image in $y = 0$ plane computed using compressive sensing and single polarization.

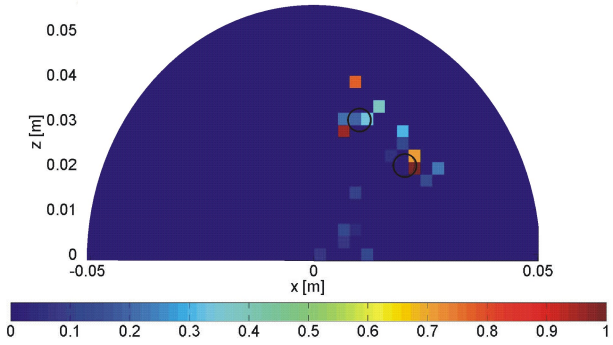

Fig. 6. Breast image in $y = 0$ plane computed using compressive sensing and dual polarization.

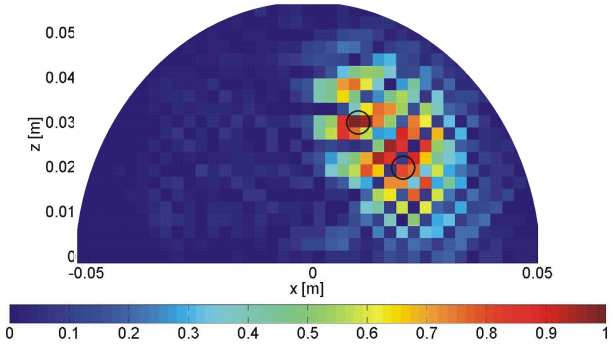

Fig. 7. Breast image in $y = 0$ plane computed using beamforming and single polarization.

IV. Conclusions

We showed that compressive sensing is an effective tool for microwave imaging of targets hidden inside dispersive homogeneous dielectric bodies. We extended the idea of sparse localization aimed for hemispherical case [16] by considering an arbitrary 3D embedding medium and by including both polarizations. We considered the breast-cancer estimation to assess the performance of the presented algorithm. In the computations, we used realistic electromagnetic models. Preliminary results showed that imposing sparseness constraint improved the image resolution and reduced blurriness, as opposed to the case in which images were obtained by beamforming. The computation load of our CS based method is higher than that of beamforming.

References

[1] E. J. Candès and M. B. Wakin, "An introduction to compressive sampling," *IEEE Signal Process. Mag.*, vol. 25, no. 2, pp. 21–30, Mar. 2008.

[2] R.G. Baraniuk, "Compressive sensing [lecture notes]," *IEEE Signal Process. Mag.*, vol. 24, no. 4, pp. 118–121, July 2007.

[3] S. Chen, D. L. Donoho, and M. A. Saunders, "Atomic decomposition by basis pursuit," *SIAM J. Sci. Comp.*, vol. 20, no. 1, pp. 33–61, 1998.

[4] E. J. Candès and T. Tao, "The Dantzig selector: Statistical estimation when p is much larger than n," *Ann. Statist.*, vol. 35, pp. 2313–2351, 2007.

[5] R. Tibshirani, "Regression shrinkage and selection via lasso," *J. Roy. Statist. Soc. Ser. B*, vol. 58, pp. 267–288.,1996.

[6] C.A. Balanis, *Advanced Engineering Electromagnetics*, John Wiley and Sons, New York 1989.

[7] P. M. Meaney, M. W. Fanning, D. Li, S. P. Poplack, and K. D. Paulsen "A clinical prototype for active microwave imaging of the breast," *IEEE Trans. Microwave Theory Tech.*, vol. 48, no. 11, pp. 1841–1853, Nov. 2000.

[8] A. E. Bulyshev, S. Y. Semenov, A. E. Souvorov, R. H. Svenson, A. G. Nazarov, Y. E. Sizov, and G. P. Tatsis "Computational modeling of three-dimensional microwave tomography of breast cancer," *IEEE Trans. Biomed. Eng.*, vol. 48, no. 9, pp. 1053–1056, Sep. 2001.

[9] Z. Q. Zhang, Q. Liu, C. Xiao, E. Ward, G. Ybarra, and W. T. Joines "Microwave breast imaging: 3-D forward scattering simulation," *IEEE Trans. Biomed. Eng.*, vol. 50, no. 10, pp. 1180–1189, Oct. 2003.

[10] E. C. Fear, X. Li, S. C. Hagness, and M. Stuchly "Confocal microwave imaging for breast cancer detection: Localization of tumors in three dimensions," *IEEE Trans. Biomed. Eng.*, vol. 49, no. 8, pp. 812–822, Aug. 2002.

[11] E. J. Bond, X. Li, S. C. Hagness, and B. D. Van Veen "Microwave imaging via space-time beamforming for early detection of breast cancer," *IEEE Trans. Antennas Propagat*, vol. 51, no. 8, pp. 1690–1705, Aug. 2003.

[12] X. Li, S. K. Davis, S. C. Hagness, D. W. van der Weide, and B. D. Van Veen "Microwave imaging via space-time beamforming: Experimental investigation of tumor detection in multilayer breast phantoms," *IEEE Trans. Microwave Theory Tech.*, vol. 52, no. 8, pp. 1856–1865, Aug. 2004.

[13] S. K. Davis, H. Tandradinata, S. C. Hagness, , and B. D. Van Veen "Ultrawideband Microwave Breast Cancer Detection:A Detection-Theoretic Approach Using the Generalized Likelihood Ratio Test," *IEEE Trans. Biomed. Eng*, vol. 52, no. 7, pp. 1237–1250, Jul. 2005.

[14] B. Kolundzija et al., WIPL-D Pro v6.1: 3D Electromagnetic Solver, Professional Edition. User's Manual, WIPL-D d.o.o., 2006.

[15] D. M. Malioutov, M. Cetin, and A. S. Willsky, "Sparse signal reconstruction perspective for source localization with sensor arrays," *IEEE Trans. on Signal Processing*, vol. 53, no. 8, pp. 3010–3022,2005.

[16] A. C. Gurbuz, J.H. McClellan, W.R. Scott, "A compressive sensing data acquisition and imaging method for stepped frequency GPRs," *IEEE Trans. on Signal Processing*, vol. 57, no. 7, pp. 2640–2650,July 2009.

[17] H. Qiong, Q. Lele Qu, W. Bingheng, F. Guangyou, "UWB Through-Wall Imaging Based on Compressive Sensing," *IEEE Trans. on Geoscience and Remote Sensing*, vol. 48, no. 3, pp. 1408–1415, Mar. 2010.

[18] L. Carin, "On the Relationship Between Compressive Sensing and Random Sensor Arrays," *IEEE Antennas and Propagation Magazine*, vol. 5', no. 5, pp. 72–81, Oct. 2009.

[19] M. Grant and S. Boyd, CVX: *Matlab software for disciplined convex programming*, http://stanford.edu/ boyd/cvx, June 2009.

[20] M. Grant and S. Boyd. *Graph implementations for nonsmooth convex programs*, Recent Advances in Learning and Control (a tribute to M. Vidyasagar), V. Blondel, S. Boyd, and H. Kimura, editors, pages 95-110, Lecture Notes in Control and Information Sciences, Springer, 2008